THE *UNIVERSITY of* EDINBURGH

Edinburgh Research Explorer

Time-Correlated Single Photon Raman Spectroscopy at MegaHertz Repetition Rates

OPEN ACCESS

Optics Letters

Time-correlated single photon Raman spectroscopy at megahertz repetition rates

Neil Finlayson,[1,*] Andrea Usai,[1] Gillian E. Brown,[1] Heather McEwan,[2] Ahmet T. Erdogan,[1] Colin J. Campbell,[2] and Robert K. Henderson[1]

[1]*Institute for Integrated Micro and Nano Systems, School of Engineering, University of Edinburgh, Alexander Crum Brown Road, Edinburgh EH9 3FF, UK*
[2]*Joseph Black Building, School of Chemistry, University of Edinburgh, David Brewster Road, Edinburgh EH9 3FJ, UK*
*Corresponding author: n.finlayson@ed.ac.uk

Significant improvements in time-correlated single photon counting (TCSPC) Raman spectroscopy acquisition times can be achieved through exploitation of megahertz (MHz) laser repetition rates. We have developed a TCSPC Raman spectroscopy system based on a high peak power (>40 W) pulsed laser, a high pulse repetition rate (40 MHz), a custom $f/1.5$ spectrometer, and a 512 spectral channel $\times$ 16 time bin single photon avalanche diode line sensor. We report millisecond Raman spectrum acquisition times, a peak Raman count rate of 104 kcps, and a linewidth aggregated count rate of 440 kcps with a diamond sample. This represents a three-order-of-magnitude increase in measured Raman count rate in comparison with a 104 kHz pulsed laser operating at 300 W and a four-order-of-magnitude increase over a 0.1 W pulsed laser operating at 40 MHz. A Raman-to-fluorescence ratio of 4.76 is achieved with a sesame oil sample at a 20 MHz repetition rate. Achieving high count rates and Raman-to-fluorescence ratios unlocks the potential of combined Raman/fluorescence lifetime spectroscopy for imaging and other short acquisition time applications. © 2021 Optical Society of America

Raman spectroscopy has established itself as an indispensable tool in chemical analysis, spanning applications from biomedicine to materials characterization. However, Raman signals are generally weak, and as Raman expands into more challenging domains such as medical imaging, there is a need to improve signal-to-noise ratios and drive down acquisition times. A significant component of the noise in Raman spectra comes from background components such as fluorescence.

Pulsed lasers used in combination with time-resolving photon detection systems can enhance Raman signal discrimination in the presence of fluorescence compared with continuous-wave (CW) techniques [1]. In recent years, time-gated [2–4] and time binning [5] single photon avalanche diode (SPAD) detectors have been used for time-correlated single photon counting (TCSPC) Raman spectroscopy (see the recent review by Kogler *et al.* [6].) Time-gating SPADs depend on activating photon detection over a time window spanning the excitation laser pulse, before most of the fluorescence signal arrives. In contrast,

time binning involves the in-pixel CMOS construction of a multiple bin histogram that counts photon time stamps during and beyond the laser time range, a technique that permits simultaneous acquisition of Raman and fluorescence signals in the same exposure [5].

Time-gated SPAD Raman acquisition times of 29 s using pulsed laser repetition rates of 350 kHz compared with 0.17 s using a conventional CW Raman system have been reported [7]. CW Raman spectrum acquisition times of less than 10 ms have been reported with high quantum efficiency electron multiplying charge coupled device detectors [8,9]. EMCCD detectors, however, do not provide fast time-gating capability to discriminate Raman signals from fluorescence.

The laser repetition rate in TCSPC sets an upper saturation limit on the Raman count rate since the number of signal photons per laser period in a given spectral channel is at most one or usually less. It is advantageous therefore to make the laser repetition rate as high as possible to maximize the detection rate [4]. Significant improvements in time-correlated single photon Raman spectroscopy acquisition times can be achieved through exploitation of high peak power and MHz laser repetition rates. To date, there is a lack of investigation on the way in which the Raman count rate responds to changes in these variables.

We can define a Raman count rate in units of counts per second (cps):

$$C = k P_p \tau f_{\text{rep}},$$

(1)

where P_p is the peak laser power (in W), τ is the laser pulse width (in s), and f_{rep} is the laser repetition rate (in Hz). k is a proportionality constant based on the following excitation, sample, collection, and detection variables [10]: laser pulse width, beam shape, differential Raman cross section, number density of scatterers, optical path length (typically the sample path length monitored by the spectrometer), sample area monitored by the spectrometer, collection solid angle of the spectrometer at the sample, transmission of the spectrometer and collection optics, quantum efficiency of the detector, and observation time.

Through rigorous investigation of repetition rate and peak power, we demonstrate Raman peak count rates of 104 kcps and millisecond spectral acquisition times in a diamond sample, thus unlocking the potential of time-resolved Raman for rapid

hyperspectral imaging and other short acquisition time applications. A 512 parallel spectral channel x 16 time bin SPAD line sensor is used for detection [11].

Four pulsed lasers were used as excitation sources in our experiments. Their characteristics are summarized in Table 1. Laser A is based on a 1064 nm gain-switched laser diode. The output is amplified in a fiber amplifier, and second harmonic conversion to a wavelength of 532 nm is carried out through a crystal in the remote head. Laser A can be operated at 1–40 MHz repetition rates and can generate peak powers of >40 W. Most of the results presented here were gathered with laser A. Lasers B and C are passively *Q*-switched microchip lasers incorporating harmonic conversion and, in the case of laser B, fiber amplification. Laser B is operated at a fixed 104 kHz repetition rate and can generate peak powers of >7 kW. Laser C is operated at a fixed 4 kHz repetition rate and can generate peak powers of >6 kW. Laser D is a picosecond laser diode operated at 40 MHz in this study and capable of 0.3 W peak power. Laser beam profile variations at the sample are likely to be significant and will be the subject of a future study.

The detection system is a 512 pixel (23.78 μm pixel pitch) TCSPC line sensor. Each pixel incorporates 16 CMOS SPADs that can be independently activated [11]. On-chip per-pixel time-to-digital converters (TDCs) and TCSPC histograms enable sensor throughput of up to 16.5 giga-events/s for time-resolved spectroscopy. Each pixel histogram includes up to 32 time bins with time bin resolutions configurable from 50 ps to 6.4 ns and time ranges from 1.6 ns to 204 ns. In histogramming TCSPC mode, the dark count rate (DCR) can be mitigated through background subtraction.

Experiments with the four lasers typically used eight activated SPADs yielding low sensor DCRs, and a 10× microscope objective having NA 0.25. Laser A experiments with 16 activated SPADS and a 20× microscope objective having NA 0.4 yielded the greatest count rates and shortest acquisition times, albeit with higher levels of DCRs that were minimized through background subtraction utilizing time bin data obtained before the rising edge of the excitation pulse.

The experimental setup is shown in Fig. 1. Both sample and detector are positioned on $x - y - z$ stages that permit transverse and longitudinal focus adjustments. The laser beam

Table 1.   Key Properties of Lasers Used in Experiments

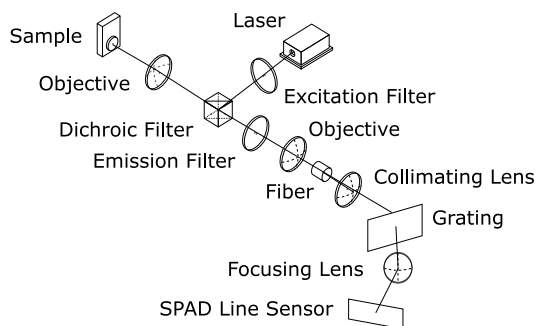| Laser	A	B	C	D
Wavelength (nm)	532	532	532	532
Linewidth (nm)	0.15	0.01	0.01	0.18
Pulse width (ps)	40	700	500	60
Typical peak power (W)	40	7143	6000	0.29
Typical average power (mW)	64	520	12	0.7
Typical pulse energy (nJ)	1.6	5000	3000	0.017
Repetition rate (MHz)	1-40	0.104	0.004	1-40

Fig. 1.   Experimental setup.

is passed through an excitation filter (SEMROCK SP01-532RU-25) and reflected by a dichroic filter (SEMROCK LPD02-532RU-25) onto the sample using 10× 0.25NA or 20× 0.4NA microscope objectives. Raman and fluorescence signals are transmitted back through the dichroic, through an ultra-steep long-pass emission filter (SEMROCK LP03-532RU-25) and coupled to a custom $f/1.5$ spectrometer through a 10× 0.25NA microscope objective and 50 μm diameter fiber optic patch cable that acts as the system pinhole. Light emerging from the other end of this fiber is collimated with an achromatic doublet lens (ThorLabs AC254-050-A-ML) and then diffracted by an 1800 lp/mm Wasatch Photonics transmissive holographic grating. Finally, the photons are focused using an achromatic doublet lens with focal length 75 mm (ThorLabs AC508-075-A-ML) and collected by the CMOS SPAD line sensor. The spectrometer spectral range is approximately 80 nm, and the spectral resolution is approximately 0.16 nm.

Spectrometer wavenumber/wavelength calibration is carried out using both TCSPC and single photon counting (SPC) signals against known standards. TCSPC Raman signals from a calcite sample are shown in Fig. 2, together with neon calibration lamp spectral peaks captured in SPC mode. Calcite Raman peak positions that match literature values [12] are overlaid onto the figure as vertical lines (156 cm^{-1}–536.5 nm, 283 cm^{-1}–540.1 nm, 713 cm^{-1}–553 nm, 1086 cm^{-1}–564.7 nm). Known neon emission spectrum peaks are also labeled with lines (576.4, 582, 585.25, 588.2, 594.5, 597.6, 602, 607.4, 609.6 nm). No relative intensity calibration of the spectrometer was carried out. A diamond sample was used to characterize the TCSPC Raman count rate as a function of laser peak power and repetition rate. Peak power levels were calibrated from average power measurements (ThorLabs PM100D power meter) and manufacturer supplied laser pulse widths.

The variation of Raman count rates with both peak power and repetition rate is demonstrated in Fig. 3. Laser A was utilized for these experiments with exposure times of 10 s.

The solid lines in Fig. 3 are least squares linear fits to the experimental data. For a given repetition rate, the count rate rises in linear proportion to peak power. The fitted slopes in turn rise in linear proportion to the repetition rate. Note that in these experiments, it is important to ensure that TDC triggering is restricted to precisely one excitation pulse per sensor delay interval; otherwise, photon time stamps can fall outside the histogram range, leading to under-counting.

Typical diamond Raman spectra obtained with each of the four lasers are presented in Fig. 4. Note that the vertical axis is on a log scale. With eight SPADs activated, the number of laser pulses required to generate a detected Raman photon were 263
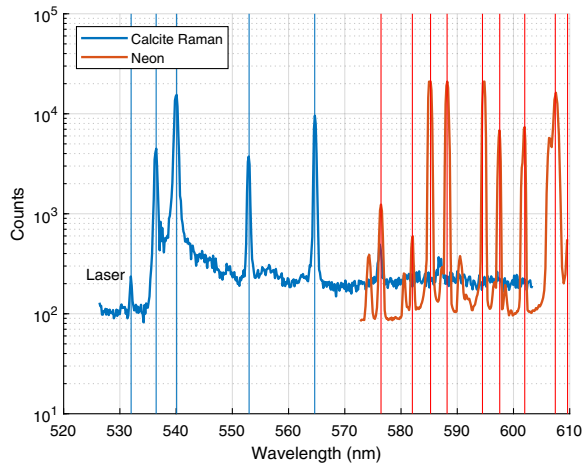
Fig. 2. Calcite time-resolved Raman peaks and neon lamp emission line peaks. The laser line is visible at 532 nm.
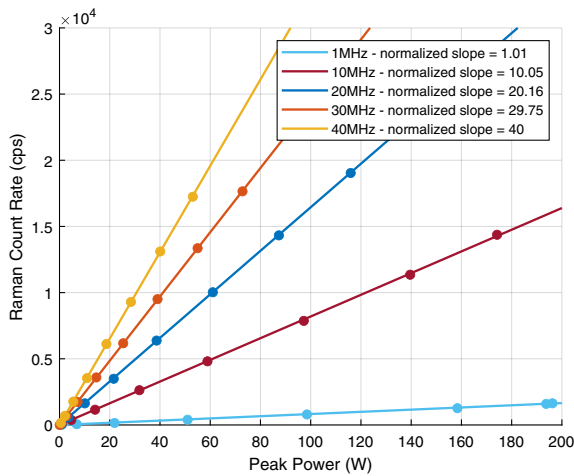

Fig. 3. Linear variation of diamond Raman count rates with laser A as a function of peak power and repetition rate. Markers show experimental results, and solid lines show least square linear fit. The fitted slopes normalized to the 40 MHz value are shown in the legend.

(laser B), 386 (laser C), 792 (laser A), and 5.9 million (laser D). On this metric, lasers B and C outperform laser A owing to high peak power levels. However, their low, fixed repetition rates result in much lower overall count rates than laser A, which has a combination of moderately high peak power and high repetition rate. Laser D has a high repetition rate, but peak power levels are too low to yield good quality Raman spectra.

Diamond has a very intense, sharp first-order Raman line at $1332 \, \text{cm}^{-1}$ arising from vibrations of the two cubic sublattices of the crystal against one another [13,14]. FWHM linewidths in each of our experimental spectra are significantly broader than quoted by Eckhardt ($3.4 \, \text{cm}^{-1}$) [13], primarily owing to limitations of our current spectrometer design. This results in diamond Raman photons being scattered into neighboring sensor pixels.

The greatest peak Raman count rate of 104 kcps was achieved with laser A operating at 40 MHz and a peak power of 53 W with 16 SPADS activated in the sensor. When counts are aggregated across neighboring pixels, the laser A 16 SPAD detection count rate rises to 440 kcps.
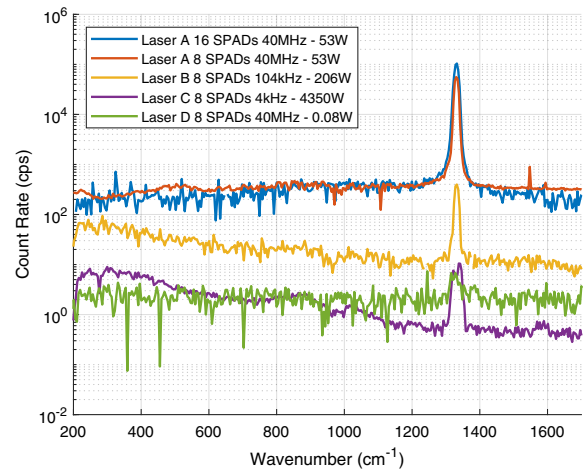

Fig. 4. Typical diamond Raman spectra obtained with each of the four lasers.

We present diamond Raman spectra obtained with short acquisition times in Fig. 5. These spectra were obtained with laser A at 40 MHz and 53 W peak power using 16 SPADs, background subtraction, and 1, 2, 5, and 10 ms exposure times.

Our results are clearly sample dependent, and diamond is an inorganic crystal with a strong Raman cross section. In fluorescence/Raman applications, a laser period of 25 ns (40 MHz repetition rate) can lead to the tail of fluorescence decay distorting the Raman signal of the subsequent pulse. In such a case, a lower laser repetition frequency may be desirable. Furthermore, a variable peak power/repetition rate system enables trade-offs between pulse energy and laser repetition rate for samples that are easily damaged by high peak power.

In Fig. 6(a), we present time-resolved spectra of sesame oil [4] obtained using laser A. Raman and fluorescence signals are captured using an exposure time of 10 s. Post-processing is restricted to background subtraction. Known sesame oil Raman peaks at 1080, 1265, 1300, 1440, 1660, and $1750 \, \text{cm}^{-1}$ are visible. Overall signal levels are greater at 40 MHz with 800 ps bins but Raman-to-fluorescence ratios are greater at 20 MHz with 100 ps time bins.

Figure 6(b) shows time-resolved signals at wavenumbers of $1440 \, \text{cm}^{-1}$ (Raman plus fluorescence) and $1500 \, \text{cm}^{-1}$
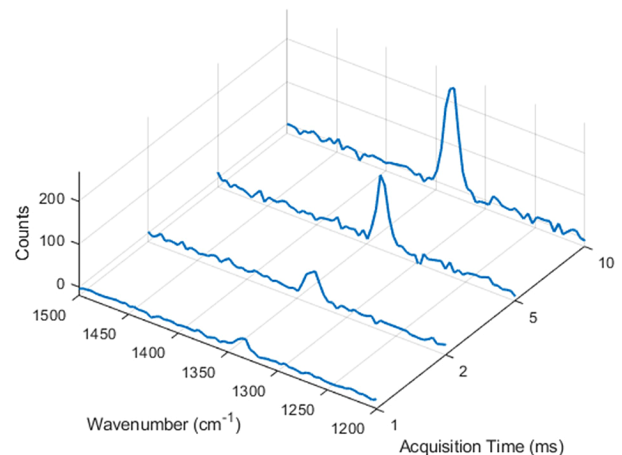

Fig. 5. Diamond Raman spectra obtained with laser A at 40 MHz and 53 W peak power using 16 SPADs and 1, 2, 5, and 10 ms acquisition times.
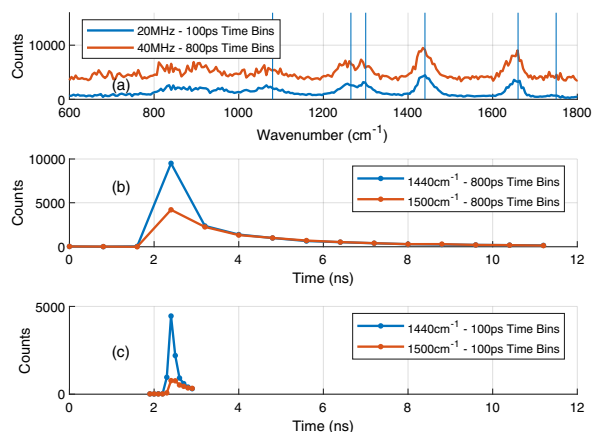
Fig. 6. (a) Sesame oil Raman-fluorescence spectra obtained with laser A at 40 MHz (800 ps time bins) and 20 MHz (100 ps time bins). (b) Raman and fluorescence time-resolved signal at 1440 cm^{-1} and background fluorescence signal at 1500 cm^{-1} (40 MHz/800 ps bins).

(fluorescence). The time origin is set to the center of the first time bin, the bin width is set to 800 ps, and on-chip delay is used to position the signal peak at 2.4 ns. The Raman plus fluorescence signal rises in a single bin, whereas fluorescence persists over a longer time interval. The fluorescence lifetime is estimated to be 2.7 ns, using a least squares single exponential fit ranging over seven time bins from the 3.2 ns position. The Raman-to-fluorescence ratio in Fig. 6(b) is 1.27. In Fig. 6(c), we utilize 100 ps bin resolution and fine (63 ps) increments of bin position using the sensor's delay generator to improve the Raman-to-fluorescence ratio. In contrast to fluorescence, the Raman signal component is essentially undelayed with respect to the excitation laser pulse [1], and therefore makes a stronger contribution at the peak bin width and position, and an improved Raman-to-fluorescence ratio of 4.76 at the 20 MHz repetition rate is achieved.

In conclusion, we have used the combination of a high peak power, MHz repetition rate laser and a high throughput histogramming TCSPC SPAD line sensor to demonstrate a peak time-resolved Raman count rate of 104 kcps, a linewidth aggre-gated count rate of 440 kcps, and acquisition times as low as 1 ms with a diamond sample. Sesame oil Raman and fluorescence lifetime signals were captured simultaneously, and an optimal combination of laser and sensor operating parameters enabled Raman-to-fluorescence ratios of 4.76 to be achieved.

REFERENCES

1. P. P. Yaney, J. Opt. Soc. Am. **62**, 1297 (1972).
2. I. Nissinen, J. Nissinen, A.-K. Lansman, L. Hallman, A. Kilpela, J. Kostamovaara, M. Kogler, M. Aikio, and J. Tenhunen, in *Proceedings of the European Solid-State Device Research Conference (ESSDERC)* (IEEE, 2011), pp. 375–378.
3. Y. Maruyama, J. Blacksberg, and E. Charbon, IEEE J. Solid-State Circuits **49**, 179 (2014).
4. T. Talala, V. A. Kaikkonen, P. Keranen, J. Nikkinen, A. Harkonen, V. G. Savitski, S. Reilly, U. Dziechciarczyk, A. J. Kemp, M. Guina, A. J. Makynen, and I. Nissinen, IEEE Trans. Instrum. Meas. **70**, 6004110 (2021).
5. A. Usai, N. Finlayson, C. D. Gregory, C. Campbell, and R. K. Henderson, in *Photonics West* (2019), paper 10873-26.
6. M. Kögler and B. Heilala, Meas. Sci. Technol. **32**, 012002 (2020).
7. J. Kekkonen, M. A. J. Finnilä, J. Heikkilä, V. Anttonen, and I. Nissinen, Analyst **144**, 6089 (2019).
8. H. Fischer, T. Dieing, and O. Hollricher, Microsc. Today **16**, 24 (2008).
9. C. Scotté, H. B. de Aguiar, D. Marguet, E. M. Green, P. Bouzy, S. Vergnole, C. P. Winlove, N. Stone, and H. Rigneault, Anal. Chem. **90**, 7197 (2018).
10. R. L. McCreery, *Handbook of Vibrational Spectroscopy*, P. R. Griffiths, ed. (Wiley, 2006).
11. A. T. Erdogan, R. Walker, N. Finlayson, N. Krstajic, G. Williams, J. Girkin, and R. Henderson, IEEE J. Solid-State Circuits **54**, 1705 (2019).
12. H. G. M. Edwards, S. E. J. Villar, J. Jehlicka, and T. Munshi, Spectrochim. Acta A **61**, 2273 (2005).
13. G. Eckhardt, D. P. Bortfeld, and M. Geller, Appl. Phys. Lett. **3**, 137 (1963).
14. C. Ramaswamy, Nature **125**, 704 (1930).